ECS Transactions, 78 (1) 1749-1758 (2017)
10.1149/07801.1749ecst ©The Electrochemical Society

Effect of YSZ Coatings as Diffusion Barrier between Glass Sealing and Steel

R. Spotorno[a], E. Fracchia[a], G. Schiller[b], P. Piccardo[a]

[a] Department of Chemistry and Industrial Chemistry, University of Genoa, Genoa, Italy
[b] German Aerospace Center, Stuttgart, Germany

In this work three experimental glass compositions have been applied and tested on ferritic stainless steel (FSS) substrates with and without yttria-stabilized zirconia (YSZ) coating deposited by plasma spraying. Samples have been tested at 780°C in static air up to 1000 hours to investigate the materials compatibility, stability and interactions at the interfaces. Microstructural changes and migration of elements have been characterized post-experiment in cross-section by means of scanning electron microscopy and energy dispersive X-ray analysis. Two of the tested compositions resulted well adherent to the metal substrate for the whole test duration and the interface evolved with the formation of a stable Cr, Mn-rich layer due to the steel oxidation. The application of YSZ allowed all the glass composition to bond to the substrate and effectively act as a diffusion barrier limiting the diffusion of the substrate elements.

Introduction

Sealant materials are needed in Solid Oxide Fuel Cell (SOFC) stacks to provide gas tightness between the fuel and oxidant compartments. Such materials therefore have to be gastight and stable under cell operating conditions without flowing or migrating from the designated sealing region. They have to be mechanically compatible with the adjoining components to avoid cracks and delamination and should withstand to thermal cycling between operational temperature and room temperature (1,2). Sealants have to form mechanically strong bonds between different stack components keeping separated the reactants. They usually join electrolyte-window frame, interconnect-window frame, interconnect-interconnect, and end plates depending on the stack design (3,4). The role of sealants becomes more and more critical when the system is constituted by a large number of cells to avoid excessive gas losses. Additionally they have to be electronically insulant to prevent short-circuits between the stack repeating units which could lead to decrease of the system efficiency and higher degradation rates of the cells (5).

Glass and glass-ceramic materials are the most common sealants for SOFC since their possibility to achieve good adhesion to the metal substrates, gas tightness, high electrical resistance, ease of fabrication and application, competitive costs (1). The selection of a glass or glass-ceramic sealant is driven by its coefficient of thermal expansion (CTE) and transition temperature (Tg). The CTE must be compatible with the other cell components such as the electrolyte and interconnect to avoid failures induced by thermal stresses. The Tg must be close to the stack operation temperature since the glass has to soften providing a proper seal but keeping at the same time a sufficient rigidity (6). Due to the

operating temperatures, reactions and diffusion processes can occur at the interfaces resulting in the formation of undesirable phases that could compromise the glass properties (7-9).

The application of a barrier layer between the two components could be indicated as suitable countermeasure avoiding the migration of elements at the interfaces (7,10). The interfacial behavior between several glass and glass-ceramics compositions with YSZ has been widely investigated being the latter the most common SOFC electrolyte material. Such studies indicated high chemical and mechanical compatibility between the two materials and stability at SOFC operating conditions (7,9-11).

In this work the barrier properties and compatibility at the interfaces of yttria-stabilized zirconia (YSZ) have been investigated. YSZ layers have been applied by means of plasma spraying on as-rolled FSS substrates. Three glass compositions, applied on substrates with and without YSZ coating, have been tested at 780°C in static air up to 1000 hours to investigate the barrier layer effects, the compatibility of the materials and stability of the interfaces. Microstructural changes and migration of elements have been characterized post-experiment in cross-section by means of scanning electron microscopy (SEM) and energy dispersive X-ray analysis (EDX).

Materials and Methods

In this study, the interaction between AISI 441 metal substrates with and without a YSZ coating with different glass compositions has been investigated. The substrates preparation consisted in cutting 10x10x0.5mm^3 AISI 441 sheets and ultrasonically cleaning (600W, 40kHz) for 5 minutes in acetone and 5 minutes in deionized water. In case of bare substrates no surface changes were applied after the cold rolling carried out by the steel producer.

The YSZ coating process was performed by Vacuum Plasma Spraying (VPS) from powders using a Triplex 200Pro Plasma Spray System by Sulzer Metco. The metallic substrates have been preheated at 400°C before the deposition. YSZ powders (8 mol% Y_2O_3 doped Zr_2O, 10-2247, Medicoat AG, Switzerland) were injected at a distance of 30 mm from the nozzle. The composition of the plasma-forming gas was 50 slpm of Ar, 1 slpm of H_2, 15 slpm of He with a current of 600 A and the pressure of the deposition chamber of 60 mbar. The nozzle-substrate distance was 300 mm and their relative velocity 320 mm/s. The incidence of the plasma jet on the metal substrate was normal and 10 layers were deposited on the substrate.

Three glass compositions, named GS-1, GS-2 and GS-3 were used in this study. Glass powders were mixed with terpineol to obtain a slurry. The powder/solvent ratio was approximately 10:1 in weight. Before the application, mixture was homogenized using a mechanical blender and treated in an ultrasonic bath to remove gas bubbles. The slurry was applied on bare and YSZ-coated AISI 441 steel substrates using a spatula to obtain homogeneous layers.

After the samples preparation, a curing thermal treatment in static air was performed. It consisted in a 1 h dwell at 400°C to allow the complete solvent removal and a joining

step of 30 minutes in the range 700-900°C depending on the glass composition. The heating rates were of 5°C min^{-1} while the cooling ramps were of 2°C min^{-1}.

The curing treatment itself is already the first part of test giving information about the compatibility of the glass with the substrate in terms of adhesion. Additional characteristics of the sample such as glass microstructure and interaction layers at the interfaces can be evaluated in order to be compared with those of samples exposed for longer testing times.

Samples were then aged up to 1000 hours in static air performing 4 cycles between room temperature and 780°C. Each cycle consisted in controlled heating/cooling ramps speed of 2°C min^{-1} to avoid thermal shocks and dwell at 780°C for 250 h. After each cycle one sample per type was extracted from the furnace for the post-experiment characterization in order to evaluate the intermediate aging stages.

For the post-experiment investigations, samples were epoxy mounted and cut to expose their cross-section. They were subsequently polished using SiC paper from 180 to 1000 grit and finished with diamond suspensions of 6, 3, 1 and 0.25 µm grain size. Before the microscopic observation, samples were coated with 5 nm of gold. Polished and coated cross-sections were examined by scanning electron microscopy (SEM, Zeiss EVO 40) equipped with an energy dispersive X-ray spectroscope (EDXS Pentafet) sensitive to light elements. In this paper the images of samples after the curing treatment, aged for 500 and 1000 hours are only shown being the most representative of the aging effects. Porosity and thickness of the YSZ layers were evaluated through image analysis (Fiji Imagej 1.47 h) on SEM micrographs.

Results

Glass-Steel Compatibility

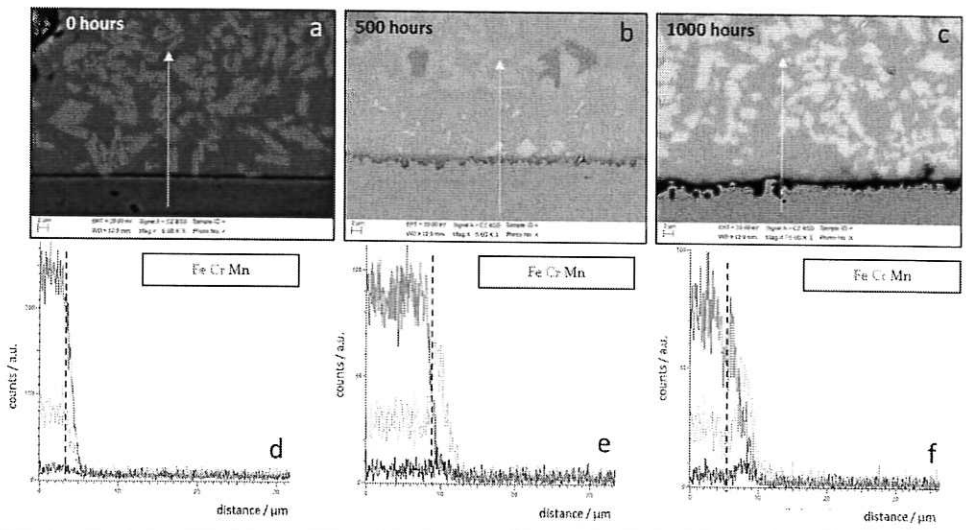

Figure 1. SEM-BSE image of the FSS/GS-1 sample cross section after the curing treatment (a), 500 hours aging (b), 1000 hours aging (c) and the respective EDX line scans along the arrow in the images (d-f). Glass-steel interface is indicated in the EDX scans by a dashed line.

The glass composition GS-1 exhibited good adhesion to the steel forming a continuous interface without any detachment (Figure 1a). The bulk of the glass was characterized by the presence of polygonal crystals homogeneously distributed along the section. After aging for 500 hours (Figure 1b), it was possible to notice the effect of the high temperature resulting in irregular interface and the formation of a dark interaction layer between the two materials and the growth of bright crystals with polygonal shape nucleating at the interface.

This study was not focused on the chemical composition of the formed phases; however the contrast of SEM backscattering electron (SEM-BSE) images depends on the elemental compositions. Bright phases result denser compared to the dark ones.

After four thermal cycles (1000 hours, Figure 1c) the glass was still well adherent to the substrate and no significant evolution of its bulk and the interaction layer were observed.

The EDX line scans (figures 1d, 1e) confirmed the oxidation of the steel substrate showing the presence of chromium and manganese peaks at the interface indicating the formation of a spinel phase. Such oxide layer evolved after 1000 h being characterized by the presence of iron (Figure 1f) coming from the substrate material.

The second glass composition, GS-2, exhibited poor adhesion to the steel after the sealing treatment (Figure 2). The glass resulted detached from the substrate and pores with distributed size were present along the whole bulk section. Compared to the first composition, high amount of crystals with smaller size were homogeneously distributed in the bulk.

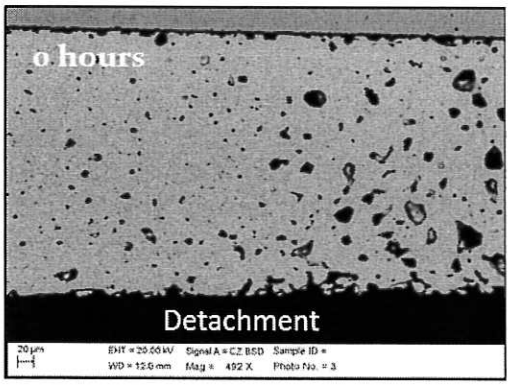

Figure 2. SEM-BSE image of the FSS/GS-2 sample cross section after the curing treatment. A porosity gradient, visible along the glass section, is likely caused by the sample preparation.

GS-3 showed a similar behavior compared to GS-1 (Figure 3a). The glass resulted well adherent to the steel after the curing treatment and polygonal crystal, homogeneously distributed, characterized the bulk section. After two thermal cycles (500 hours, Figure 3b), dark crystals were found in the bulk while bright crystals nucleated at the interface with the steel.

High temperature corrosion of the steel was observed resulting in the formation of dark oxides localized within the metal, near to the surface. As a consequence of it, chromium migrated toward the glass forming a dark layer at the interface. Such layer evolved increasing its thickness up to 1000 hours of ageing while the oxide particles within the steel grew in their diameter (Figure 3c). Also the bulk morphology changed after 4 thermal cycles exhibiting the formation of bright needle-like crystals overlapping with the dark ones. The EDX line scans showed lower interaction between the glass and the steel compared to GS-1 (Figure 3d-e). The interaction layer was thinner and the interface resulted more regular compared to GS-1 sample. Such differences could be due to the reduced corrosion of the steel. Additionally, the chromium peak at the steel/glass interface was not clearly visible for all the samples and no iron migration was observed up to 1000 hours of aging.

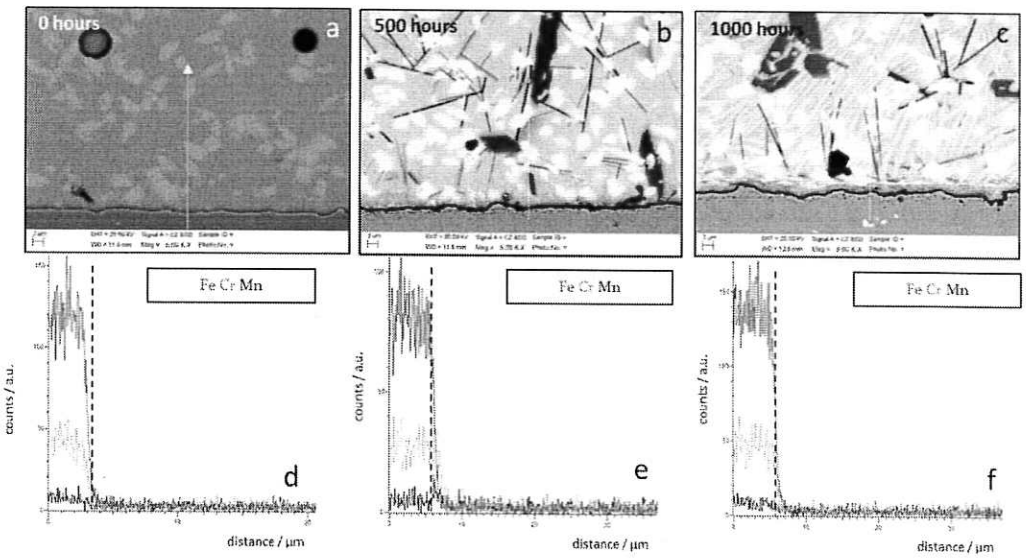

Figure 3. SEM-BSE image of the FSS/GS-3 sample cross section after the curing treatment (a), 500 hours aging (b), 1000 hours aging (c) and the respective EDX line scans along the arrow in the images (d-f). Glass-steel interface is indicated in the EDX scans by a dashed line. The EDX line scans do not give any information about the oxidation state of the elements.

YSZ Layer Characterization

Between the steel and YSZ plasma sprayed layer an oxide scale was visible, which evolved during the aging steps. Such film was mainly constituted by Cr, Mn, Fe, Al and it was already present after the YSZ layer deposition due to the temperatures involved in process. The evolution of such layer resulted not dependent by the glass composition. In Figure 4a are shown the thicknesses of the oxide scale measured in samples with GS-1 after each thermal cycle. Despite the large error bars, due to the inhomogeneity of the oxide scale, it was possible to identify an increasing trend of its thickness in the first 750 hours and then a stabilization up to 1000 hours.

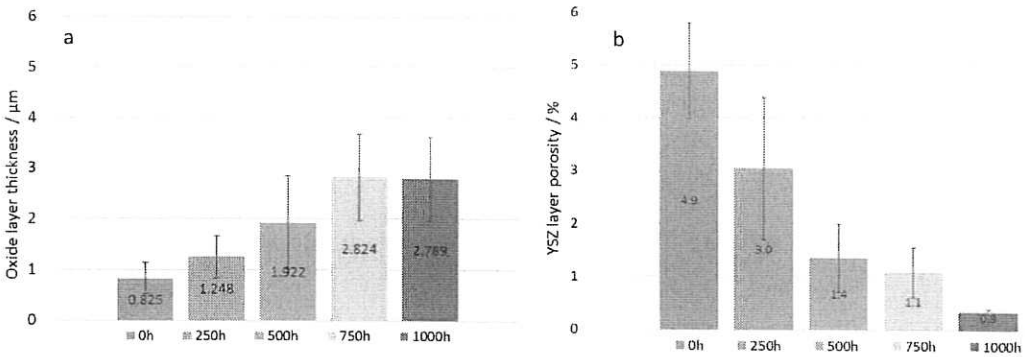

Figure 4. Thickness of the oxide layer between the steel and YSZ (a) and porosity of the YSZ layer (b)

The porosity of the YSZ layer, measured for the samples with GS-1, is shown in Figure 4b. Such feature evolved as a consequence of the aging treatment staring by initial values of 5%. As visible in figures 5-7, voids of distributed sizes were present through the whole layer sections. The high temperatures characterizing the aging treatments caused a fast decrease of the porosity in the first 500 hours and the achievement of a minimum of 0.3% after 1000 hours.

Glass-YSZ Compatibility

The application of GS-1 on YSZ resulted in good adhesion after the sealing process with the formation of an amorphous interaction layer at the glass-YSZ interface (Figure 5a). The bulk of the glass resulted not affected by the presence of the barrier layer and its evolution is coherent with the results observed in the glass-steel samples. After four thermal cycles (1000 hours, Figure 5c), a crack is visible at the YSZ-glass interface. The

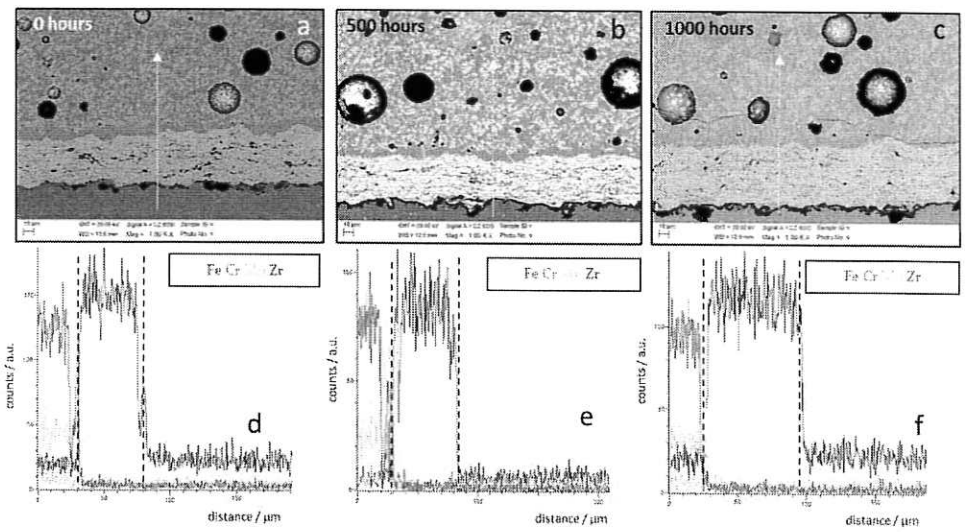

Figure 5. SEM-BSE image of the FSS/YSZ/GS-1 sample cross section after the curing treatment (a), 500 hours aging (b), 1000 hours aging (c) and the respective EDX line scans along the arrow in the images (d-f). Steel-YSZ and YSZ-glass interfaces are indicated in the EDX scans by dashed lines.

EDX analysis (figures 5d-f) showed the effectiveness of the YSZ layer in confining the element diffusion at the steel-YSZ interface. No presence of metal substrate elements was detected in the glass material.

The YSZ coating allowed the glass composition GS-2 to adhere to the substrate acting as compatibility layer between the two materials (Figure 6a). In this case, no interaction layer was visible between YSZ and the glass, which crystallinity, already high after the curing treatment, strongly increased after the first aging steps. A crack is visible in the 0 hours sample, however up to 1000 hours the glass was still adherent to the substrate and no cracks were detected (Figure 6a-c). The EDX analysis (Figure 6d-f) shows the element diffusion at the steel-YSZ interface consisting in the formation of a confined Fe-rich layer.

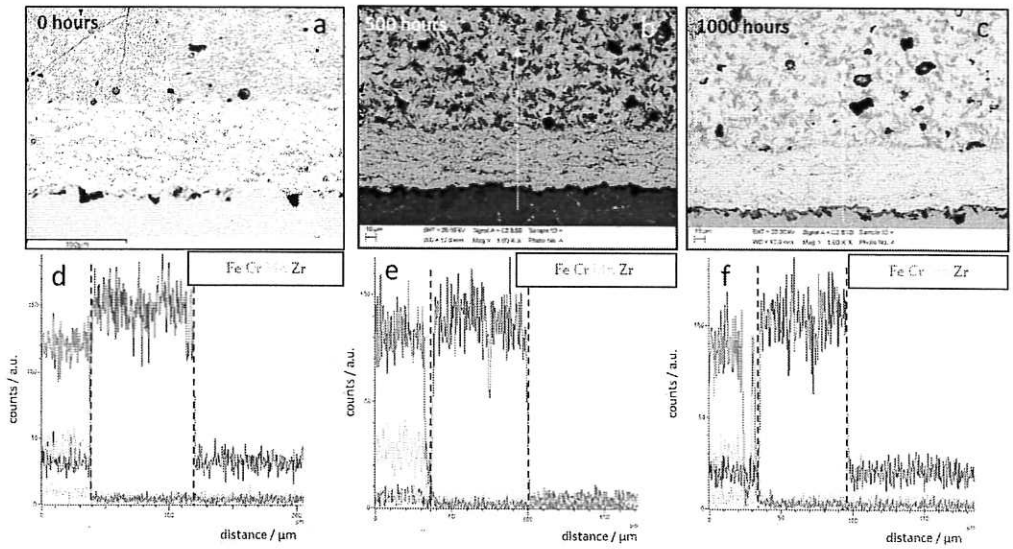

Figure 6. SEM-BSE image of the FSS/YSZ/GS-2 sample cross section after the curing treatment (a), 500 hours aging (b), 1000 hours aging (c) and the respective EDX line scans along the arrow in the images (d-f). Steel-YSZ and YSZ-glass interfaces are indicated in the EDX scans by dashed lines.

The composition GS-3 exhibited a similar behavior to the GS-1 in contact with the YSZ layer being well adherent to the substrate and forming an interaction layer at the interface between the two materials (Figure 7a).

The bulk was not affected by the presence of the barrier layer showing a coherent behavior with that observed for the glass-steel sample consisting in the nucleation and growth of additional crystalline phases as result of the aging treatment up to 1000 hours (Figure 7b, c). The adhesion of the glass to the substrate was stable for the whole test duration and no cracks in the cross section were detected. The beneficial effect of the YSZ barrier layer was confirmed by the EDX line scans also in this sample (Figure 7d-e).

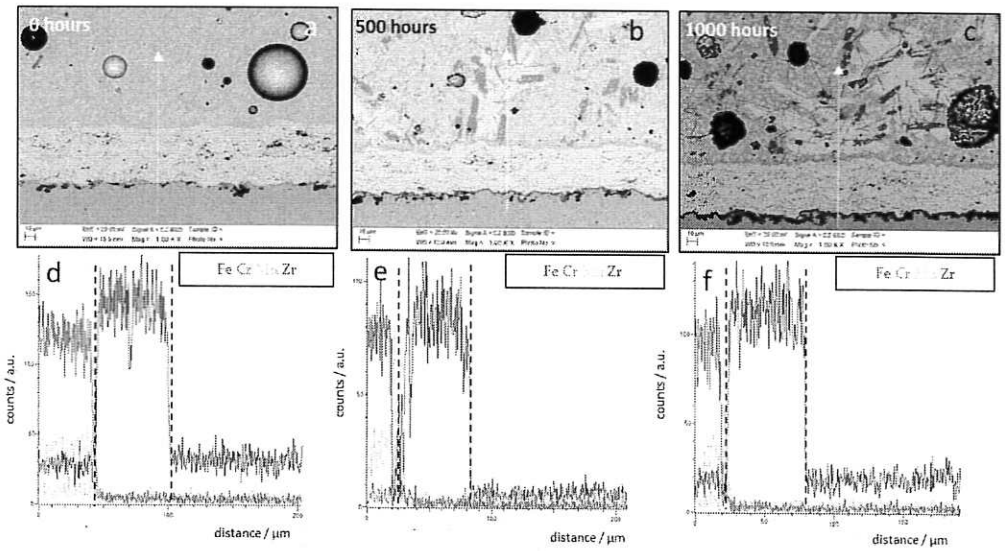

Figure 7. SEM-BSE image of the FSS/YSZ/GS-3 sample cross section after the curing treatment (a), 500 hours aging (b), 1000 hours aging (c) and the respective EDX line scans along the arrow in the images (d-f). Steel-YSZ and YSZ-glass interfaces are indicated in the EDX scans by dashed lines.

Discussion

The achievement of bonding between glass and steel for GS-1 and GS-3 indicates good mechanical compatibility and wetting properties. However, such characteristics should not be completely excluded for GS-2, which lack of adhesion could be caused by poor flow and wetting due to strong crystallization. The thermal cycle used for this composition could have not guaranteed the proper fluidity to the glass preventing the bonding to the steel. A preoxidation treatment could promote the adhesion between the two materials forming a Cr-rich oxide layer on the metal substrate with higher compatibility with the glass (8, 12).

GS-2 was also characterized by a distributed porosity along the section which, being constituted by close pores should not compromise the tightness of the seal. Porosity can be limited by adjusting the powder/binder ratio during the sample preparation or by adding a mechanical load on top of the sample to help the removal of the binder during the curing thermal treatment. As expected, for all the compositions, the crystallinity increased (6, 7, 10, 13) as effect of the aging treatment. The composition GS-3 showed the formation of additional crystalline phases characterized by sharper shapes. No negative effects were observed as consequence of the increase of crystallinity and the formation of such new phases. The glass resulted well adherent for the whole aging duration without formation of cracks or delamination.

The interfaces were characterized by the presence of a chromium-rich layer resulted by the high temperature corrosion of the steel. Such material is known to form passive Cr, Mn spinels in oxidizing environments (14-16). Despite the spinel stability, at SOFC working temperatures, iron diffused at the interface doping the oxide layer while Cr further migrated forming crystals at the interface with the glass. The spinel oxide layer

was formed also at the FSS/YSZ interface reaching a stable thickness after 750 hours of aging. The same behavior as for the FSS/glass interface was observed with an enrichment of iron. Aluminum was present in such layer as a consequence of the sandblasting treatment prior to the plasma spraying process.

The thickness of the deposited layer resulted inhomogeneous but not affecting the glass adhesion and the coating stability. The close porosity present along the YSZ layer should not affect the gas tightness of the coating and, as a result of the aging temperature, a constant decrease of it was observed. The defects detected in the YSZ layer are mainly due to inhomogeneity in the heat transfer or stresses developed during the deposition process such as hindered thermal contraction of the splats by the underlying solid (17). Despite the YSZ coating morphology, EDX analysis confirmed its beneficial effect blocking the substrate element diffusion being confined at the FSS/YSZ interface.

All the compositions resulted well adherent to the YSZ coating. The improved wetting properties of GS-2 compared to what observed with FSS, highlights the higher affinity between the two materials. The interaction layer formed at the interface resulted stable for the whole aging time and no defects originated from such interface. There is no evidence about the origin of the cracks present in GS-1 after 1000 hours and GS-2 after curing being defects visible only in such samples. However, their path, crossing large pores, suggests that they originate from the post-experiment sample preparation procedure.

Conclusions

Three glass compositions were applied on FSS substrate with and without a plasma sprayed YSZ coating. Aging tests were conducted at 780 °C in static air for four consecutive thermal cycles of 250 hours in order to investigate the effect of such conditions on the microstructures and interfaces. Two compositions resulted well adherent to the metal substrate for the whole test duration and a layer constituted by Cr, Mn, Fe was detected at the steel/glass interface. Despite the increase in crystallinity and the formation of new phases, no negative consequence or defect formation were observed up to 1000 hours.

YSZ layers resulted porous and irregular in their thickness, however the porosity decreased as effect of the thermal aging and the presence of the coating enhanced the glass/substrate compatibility allowing the GS-2 composition to adhere. Additionally, the effectiveness of the YSZ layer as diffusion barrier was confirmed detecting a confined chromium-rich oxide at the steel/YSZ interface without further diffusion of substrate elements through the coating. Concluding, GS-1 and GS-3 can be indicated as valid compositions for sealing planar stainless steel based SOFCs considering their mechanical compatibility with the steel, stability at high temperature and limited interaction with the substrate. The application of YSZ coating enhances the sealing adhesion to the substrate and constitutes a further protection of the glass confining the substrate elements diffusion.

Acknowledgments

The authors like to thank SCHOTT AG for providing the glass samples. The research leading to these results has received funding from the European Union's Seventh

Framework Program (FP7/2007- 2013) Fuel Cells and Hydrogen Joint Undertaking (FCU-JU-2013-1) under grant agreement No 621207.

References

1. M. K. Mahapatra and K. Lu, *J. Power Sources* **195**, 7129 (2010).
2. K. C. Wincewicz and J. S. Cooper, *J. Power Sources* **140**, 280 (2005).
3. P. Piccardo, A. Pecunia, V. Bongiorno, R. Spotorno, Z. Wuillemin and J. P. Ouweltjes, *ECS Trans.* **68**, 2611 (2015).
4. Y.S. Chou, J.W. Stevenson and J. -P. Choi, *Int. J. Appl. Ceram. Technol.* **123**, 1 (2010).
5. J. F. B. Rasmussen, P. V. Hendriksen and A. Hagen, *Fuel Cells* **8**, 385 (2008).
6. J. W. Fergus, *J. Power Sources* **147**, 46 (2005).
7. Y. -S. Chou, E. C. Thomsen, J. -P. Choi and J. W. Stevenson, *J. Power Sources* **202**, 149 (2012).
8. F. Hong and D. Holland, *Journal of Non-Crystalline Solids* **112**, 357 (1989).
9. F. Smeacetto, M. Salvo, M. Ferraris, J. Cho and A. R. Boccaccini, *Journal of the European Ceramic Society* **28**, 61 (2008).
10. Y. -S. Chou, E. C. Thomsen, J. -P. Choi and J. W. Stevenson, *J. Power Sources* **197**, 154 (2012).
11. F. Smeacetto, M. Salvo, M. Ferraris, V. Casalegno, P. Asinari and A. Chrysanthou, *Journal of the European Ceramic Society* **28**, 2521 (2008).
12. F. Smeacetto, M. Salvo, M. Ferraris, V. Casalegno and P. Asinari, *Journal of the European Ceramic Society* **28**, 611 (2008).
13. S. T. Reis, M. J. Pascual, R. K. Brow, C. S. Ray and T. Zhang, *Journal of Non-Crystalline Solids* **356**, 3009 (2010).
14. R. Spotorno, P. Piccardo and F. Perrozzi, *ECS Trans.* **68**, 1633 (2015).
15. P. Piccardo, S. Anelli, V. Bongiorno, R. Spotorno, L. Repetto and P. Girardon, *Int. J. Hydrogen Energy* **40**, 3726 (2015).
16. V. Bongiorno, P. Piccardo, S. Anelli and R. Spotorno, *Acta Metall. Sin. (Engl. Lett.)* (2017) doi:10.1007/s40195-017-0543-1
17. R. Spotorno, P. Piccardo, F. Perrozzi, S. Valente, M. Viviani and A. Ansar, *Fuel Cells* **15**, 728 (2015).